
22 Feb 2022

Computational Study on the Microscopic Adsorption Characteristics of Linear Alkylbenzene Sulfonates with Different Chain Lengths on Anthracite Surface

Xuanlai Chen

Guochao Yan

Guang Xu

Missouri University of Science and Technology, guang.xu@mst.edu

Xianglin Yang

et. al. For a complete list of authors, see https://scholarsmine.mst.edu/min_nuceng_facwork/1648

Follow this and additional works at: https://scholarsmine.mst.edu/min_nuceng_facwork



Part of the [Chemistry Commons](#), and the [Mining Engineering Commons](#)

Recommended Citation

X. Chen et al., "Computational Study on the Microscopic Adsorption Characteristics of Linear Alkylbenzene Sulfonates with Different Chain Lengths on Anthracite Surface," *Journal of Chemistry*, vol. 2022, article no. 5318906, Hindawi, Feb 2022.

The definitive version is available at <https://doi.org/10.1155/2022/5318906>



This work is licensed under a [Creative Commons Attribution 4.0 License](#).

This Article - Journal is brought to you for free and open access by Scholars' Mine. It has been accepted for inclusion in Mining Engineering Faculty Research & Creative Works by an authorized administrator of Scholars' Mine. This work is protected by U. S. Copyright Law. Unauthorized use including reproduction for redistribution requires the permission of the copyright holder. For more information, please contact scholarsmine@mst.edu.

Research Article

Computational Study on the Microscopic Adsorption Characteristics of Linear Alkylbenzene Sulfonates with Different Chain Lengths on Anthracite Surface

Xuanlai Chen ¹, Guochao Yan ¹, Guang Xu,² Xianglin Yang,³ Jinfa Dong,¹ Zidong Liang,¹ and Shuai Wei⁴

¹School of Mining Engineering, Taiyuan University of Technology, Taiyuan 030024, China

²Department of Mining Engineering, Missouri University of Science and Technology, Rolla, MO 65409, USA

³Hunan Provincial Key Laboratory of Fine Ceramics and Powder Materials, School of Materials and Environmental Engineering, Hunan University of Humanities, Science and Technology, Loudi 417000, China

⁴Taiyuan Research Institute Co., Ltd., China Coal Technology & Engineering Group, Taiyuan 030006, China

Correspondence should be addressed to Guochao Yan; yanguochao@tyut.edu.cn

Received 28 December 2021; Revised 20 January 2022; Accepted 26 January 2022; Published 22 February 2022

Academic Editor: Mohd. Sajid Ali

Copyright © 2022 Xuanlai Chen et al. This is an open access article distributed under the Creative Commons Attribution License, which permits unrestricted use, distribution, and reproduction in any medium, provided the original work is properly cited.

In order to explore the influence of different lengths of hydrophobic carbon chains on the diffusion characteristics of surfactants on the surface of anthracite, six linear alkyl benzene sulfonates with different hydrophobic carbon chain lengths were selected (mC , $m = 8, 10, 12, 14, 16, 18$; m represents the numbers of carbon atoms in the hydrophobic carbon chain), and molecular dynamics (MD) simulations were adopted. Models of surfactant-anthracite, surfactant-graphite layer, and water-surfactant-anthracite were constructed. After analyzing a series of properties such as adsorption energy, diffusion coefficient, radial distribution function (RDF), and hydrophobic tail order parameters, it was found that 12C had the highest adsorption strength on the surface of anthracite; the reason was that 12C had the highest degree of aggregation near the oxygen-containing functional groups on the surface of anthracite. Further studies had found that the hydrophobic tail chain of 12C had the strongest isotropy. The study fills the gap in the systematic study of the diffusion characteristics of linear alkylbenzene sulfonates (LAS) with different chain lengths on the surface of anthracite, enriches and develops the basic theory of coal wettability, and also provides technical ideas for the design of new surfactants and new dust suppression agents.

1. Introduction

Surfactants are amphiphilic compounds that contain both hydrophilic and hydrophobic groups. This special structure makes it one of the most versatile chemical products [1–8] (e.g., in the oil industry, cosmetics, coal industries, and polymer paint). In recent years, surfactants have also been widely used in high-tech fields. Such as electronic printing, microelectronics technology, nanomaterials, and biopharmaceutical research [9–17]. From the overall consumption of global surfactants, the consumption of anionic surfactants is the largest [18]. From the aspects of surfactant applicability, cost performance, and overall consumption

level, anionic surfactant linear alkylbenzene sulfonates (LAS) are the most important surfactant series in the world [19–22].

LAS consists of a hydrophobic linear alkyl chain and a hydrophilic sulfonate group, which are, respectively, connected to the 1, 4 positions of the benzene ring [23]. Commercial LAS surfactants are usually complex mixtures of homologs [24] (i.e., different lengths of the alkyl chain). Heterogeneous components improve performance, making LAS widely used in different industries, such as cosmetics, detergents, and mineral extraction [25–28]. However, this heterogeneity also makes it more complicated to clarify the detailed functions of the pure LAS. So far, LAS mixtures have

been extensively studied [29–33], but systematic studies on pure LAS are relatively rare.

Surfactants have been widely used in the coal industry, such as in the fields of coal flotation and coal dust suppression [34–41]. The research on the interface characteristics of coal relies on the basic theory of coal wettability [42–44]. A large number of experimental studies have shown that the surface active agent diffusion characteristics on the coal surface determine the wetting effect of coal [45–50]. However, the experimental methods have defects in explaining the structural changes, dynamics, and energy characteristics of the molecular adsorption process on the mineral surface.

With the development of science and technology, it is becoming a reality to use computer simulations to explain the macroscopic properties from a microscopic point of view [51–59]. In particular, MD simulation has proven to be a useful tool for analyzing coal interface properties at the molecular level [60–66]. Traditional experiments screen flotation agents and dust suppression agents by trial-and-error method. MD simulation can screen agents in batches more efficiently, save a lot of time and materials, and also help to understand the adsorption mechanism from a molecular perspective. So far, researchers have conducted a large number of MD simulation studies on the diffusion characteristics of surfactants on the coal surface [44, 67–71]. However, there are few researches on the diffusion characteristics of LAS on coal surface; moreover, there is a lack of research on the mechanism and structure of the chain length in the adsorption process. We studied the adsorption characteristics of the four isomers of the linear alkylbenzene sulfonate family (LAS) on the coal surface and systematically compared the adsorption characteristics and microscopic adsorption mechanism of the LAS family members on the coal surface. [71].

In the existing research on the influence of different hydrophobic tail chain length on the properties of surfactants, researchers mostly choose two or three surfactants to compare; most of the conclusions drawn are that various properties change linearly as the length of the hydrophobic alkyl chain changes [46]. We think this is unreasonable, because the selected types of surfactants are too few to get a comprehensive conclusion. Therefore, in this study, we selected six surfactants with hydrophobic chain length $m = 8, 10, 12, 14, 16, 18$ for research. Since the LAS with even number of carbon atoms in the hydrophobic chain are more widely used and the odd-even effect [72] causes a large difference between the odd-numbered carbon atoms and the even-numbered carbon atoms, we selected the LAS with even number of carbon atoms in the hydrophobic tail chain for research. As far as we know, this is the first attempt to systematically study and compare the diffusion characteristics of LAS family members with different carbon chain lengths on the surface of anthracite.

Surfactants with different hydrophobic chain lengths have different properties, which arouses the interest of a wide range of researchers. Acisli et al. [73] studied the adsorption capacity of five cationic surfactants with different hydrophobic chain lengths on montmorillonite and found that the hydrophilicity decreased with the increases of chain

length. Ren et al. [74] study the adsorption behavior of different chain lengths Gemini surfactants on methyl orange and find that, with the increase of the chain lengths, the interlayer spacing, hydrophobicity, and dispersibility of organoclay increase significantly. Kun et al. [75] study the hydrophobic effect of three cationic surfactants with different hydrophobic chain lengths on bovine serum albumin and find that the initial step of the interaction is to attach the nonpolar carbon chain of the surfactant to the nonpolar region of the protein. Jiang et al. [76] study the effect of carbon chain lengths on the surface properties of salt-free cationic surfactants and conclude that the longer the hydrocarbon chain, the greater the hydrophobic effect. Díez-Pascual et al. [77] study the influence of surfactants with different chain lengths on the morphology of graphene and find that the thickness of the graphite flakes increases with the increase of the surfactant chain length, and the longer the molecular chain, the higher the surface coverage. Zhang et al. [78] use two Gemini surfactants (only the length of the hydrophobic tail is different) to study the adsorption of emerging pollutants after modified montmorillonite and find that an increase in the alkyl chain lengths can increase the mobility of molecules. Badache et al. [79] study the effects of different hydrophobic tail chain lengths on the interfacial properties of cationic surfactants and find that the surfactant with the longest chain has the lowest critical micelle concentration.

MD simulation was used for the calculation. Firstly, a binary system of surfactant-anthracite was constructed. The adsorption energy and diffusion coefficient of six LAS with different chain lengths were compared; a macroconclusion was drawn that the adsorption effect of 12C on the surface of anthracite was the best. Secondly a binary system of surfactant-graphite layer was constructed. Through coordination number and radial distribution function analysis, the microscopic reason for the highest adsorption strength of 12C was explained from the perspective of functional groups. In order to detect the tightness of the surfactant adsorption layer, a water layer was added to construct a water-surfactant-anthracite ternary system. Through the analysis of the RDF between oxygen atoms in the water and the order parameters of the hydrophobic tail chain, it was proved that the layer composed of 12C was the densest and had the strongest ability to “isolate” water molecules. This research fills the gap in the systematic study of the diffusion characteristics of LAS with different chain lengths on the surface of anthracite, expands the basic theory of wettability, and also provides ideas for the design and development of surfactants with new structures and new dust suppression agents.

2. Materials and Methods

2.1. Materials. This study selected the Jincheng anthracite that we had studied before (from the no. 3 coal seam of the Zhaozhuang coal mine in Jincheng). After hand-selecting and stripping the vitrinite, it was crushed and ground and passed through a 200-mesh sieve. The demineralized coal was obtained by pickling with HCl-HF-HCl. Carbonate, phosphate, clay,

silica, and other minerals in coal were removed. The acid-treated coal sample was washed with excess distilled water until the pH of the filtrate became neutral. By measuring proximate analysis, ultimate analysis, carbon nuclear magnetic resonance (^{13}C -NMR), high-resolution transmission electron microscopy (HRTEM), infrared spectroscopy (FTIR), and X-ray photoelectron spectroscopy (XPS), a molecular model of the average structural unit of Jincheng anthracite was initially constructed. Table 1 shows the results of proximate and ultimate analysis of Jincheng anthracite [80].

Analyzing the carbon skeleton parameters obtained from the ^{13}C -NMR test results of demineralized coal, it was found that the bridge carbon and the peripheral carbon were relatively high. This indicated that the degree of condensation of the benzene ring of coal molecules was relatively high. Therefore, the aromatic structure of Jincheng anthracite was dominated by fused-ring aromatic hydrocarbons formed by seven benzene rings, and the degree of substitution of aromatic rings was relatively high. Table 2 shows the structural parameters of Jincheng anthracite samples. Combining the analysis of coal samples with FTIR and XPS [80], Jincheng anthracite contained less nitrogen and exists in the form of organic nitrogen and inorganic nitrogen; the sulfur in coal samples mainly existed in the form of organic sulfur, with less inorganic sulfur. The oxygen content in coal was less in the aromatic structure, and the oxygen-containing functional groups included hydroxyl and ketone groups. Finally, two structural units S1 and S2 containing hydroxyl group and ketone group were constructed (Figure 1(a)). The surfactant molecules used in this study were six kinds of LAS with different carbon chain lengths (denoted by $m\text{C}$, where m represents the number of carbon atoms in the tail chain, $m=8, 10, 12, 14, 16, 18$); they were sodium octaalkylbenzene sulfonate, sodium decylbenzene sulfonate, sodium dodecylbenzene sulfonate, sodium tetradecylbenzene sulfonate, sodium cetylbenzene sulfonate, and sodium octadecylbenzene sulfonate. The reason for selecting them was that the six surfactants had the same hydrophilic head group, but the hydrophobic tail chain length was different. We used the controlled variable method to study the effect of surfactant tail chain length on adsorption characteristics.

x_b is the average value of the ratio of bridge carbon to peripheral carbon of aromatic compounds in coal (referred to as bridge carbon ratio); this value can reflect the degree of polycondensation of aromatic compounds, that is, the size of the aromatic nucleus. C represents the average number of carbon atoms in the aromatic layer. $\sigma + 1$ represents the average number of bridge bonds and side chains contained in each aromatic layer. P_0 represents the percentage of bridge. B.L. represents the number of bridges and rings in each aromatic layer. S.C. represents the number of side chains in each aromatic layer. MW represents the average molecular mass of the aromatic layer. $M\sigma$ represents the average molecular mass of the side chain or 1/2 bridge chain.

2.2. Computer Simulation Details. In this study, we used the molecular structure of Jincheng anthracite proposed earlier by our team to build a coal model [80], as shown in Figure 1(a). Forty optimized coal molecules (ratio 1 : 1) were

randomly stacked in a cubic unit cell ($35 \times 35 \times 35 \text{ \AA}^3$) through the Amorphous Cell module of Materials Studio 6.0. Annealing algorithm was used to relax the coal structure. The initial temperature of anthracite cell was set to 298K and then rose once every 50K until the temperature reached 1098K. Five annealing cycles were performed, and the final temperature was 298K [67, 81]. On the top of the coal seam, a 12 nm thick vacuum layer was added to prevent the influence of periodic boundary conditions. Figure 2 shows the constructed anthracite surface model.

Surfactant-anthracite, surfactant-graphite layer, and water-surfactant-anthracite system models were constructed. 10 surfactant molecules made up the surfactant layer, while 1000 water molecules made up the water layer. The length and width of the surfactant layer and the water layer are consistent with the coal model, both being 35 Å. In this way, the models can be matched when constructing surfactant-coal and water-surfactant-coal systems. The intermolecular interaction was described by the polymer uniform force field. Before the MD simulation, geometric optimization was used to minimize the energy of all models. Subsequently, NVT ensemble (the constant-temperature, constant-volume ensemble) was used for MD simulation. Nose was used for thermostat [82, 83]. The time step was set to 1 fs. 1000 ps simulations were conducted to make the systems interact with each other fully. In all MD simulations, the Ewald algorithm was selected for long-range electrostatic interaction, and the accuracy was 0.001 kcal/mol, and the atom based algorithm was selected for the van der Waals interaction, and the cut-off distance was 1.25 nm. A 12 nm vacuum layer was added to the surface of each model to eliminate the mirror effect [84]. In the display of all models, the sodium atoms were hidden to show the adsorption form of surfactants more clearly.

3. Results and Discussion

3.1. Surfactant-Anthracite System. The surfactant layer was first placed on the surface of the anthracite with the build layer tool, and the MD simulation of 1000 ps was performed. Under the action of van der Waals force and electrostatic force, the surfactant layer kept approaching the anthracite coal and finally completed the adsorption. The final adsorption configuration is shown in Figure 3. In order to highlight the adsorption form of surfactants, the coal surface model was displayed in a line model, and the surfactant was displayed in a CPK mode. The initial configuration can be viewed in the support material, as shown in Figures S1–S6.

3.1.1. Adsorption Energy. The magnitude of the adsorption energy value can measure the adsorption strength. The more negative the adsorption energy, the more energy released, the higher the degree of aggregation, and the higher the adsorption strength [37, 85, 86]. The adsorption energy is calculated by the following equations:

TABLE 1: Proximate and ultimate analysis of Jincheng anthracite.

Proximate analysis (%)				Ultimate analysis (%)				
M_{ad}	A_d	V_{daf}	FC_d	C	H	O	N	S
0.66	23.05	12.86	67.05	91.51	3.89	2.10	1.71	0.79

M_{ad} : moisture content on an air-dried basis. A_d : ash content on dry basis. V_{daf} : volatile content (in ash-free form). FC_d : fixed carbon content.

TABLE 2: Molecular structural parameter of JC anthracite coal sample.

x_b	C	$\sigma + 1$	P_0	B.L.	S.C.	MW	M_σ
0.46	27	3.0	0.40	1.2	1.8	398	20

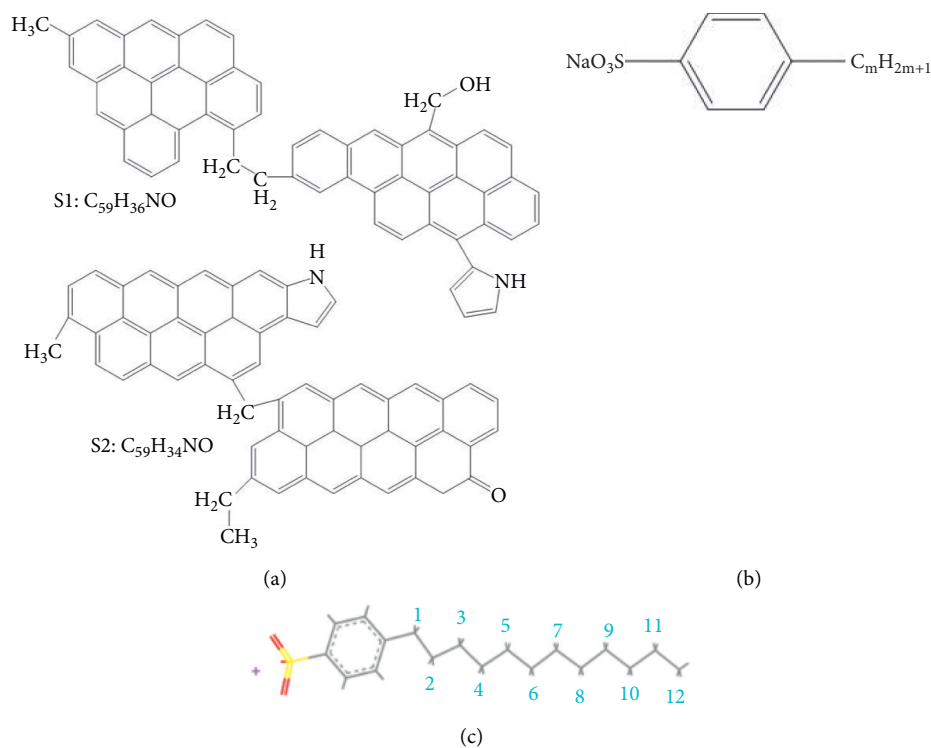


FIGURE 1: (a) Molecular structures S1 and S2 of Jincheng anthracite. (b) Linear alkylbenzene sulfonates with different hydrophobic carbon chain lengths ($m = 8, 10, 12, 14, 16, 18$). (c) Sodium dodecylbenzene sulfonate when $m = 12$.

$$\begin{aligned}
 EV &= EV_{\text{total}} - EV_{\text{coal}} - EV_{\text{surf}}, \\
 EL &= EL_{\text{total}} - EL_{\text{coal}} - EL_{\text{surf}}, \\
 E &= EV + EL,
 \end{aligned}
 \tag{1}$$

where EV stands for van der Waals adsorption energy, EL stands for electrostatic adsorption energy, E stands for total adsorption energy, E_{total} stands for the total energy of surfactant and anthracite, E_{coal} is anthracite energy, and E_{surf} stands for surfactant energy.

We use a Perl script to extract the energy directly. The average of the last 10 conformational energies was calculated to arrive at the data in Table 3. Comparing the total adsorption energy data from Table 3, the 12C-anthracite system's energy was the lowest, indicating that the 12C released the most energy during the adsorption process, the

adsorption strength was the highest, and the degree of aggregation on the anthracite coal surface was the highest. This was due to the different molecular structure of surfactants. These six surfactants had the same polar head group and different hydrophobic tail chain length. When the hydrophobic chain length m increased from 8 to 12, the hydrophobic interaction between the hydrophobic tail chain and the anthracite was enhanced, and it was easy to self-aggregate. At this time, due to the short length of the hydrophobic tail chain, the steric hindrance effect was not obvious yet (the steric hindrance effect mainly refers to the steric hindrance caused by the proximity of certain groups in the molecule; it is a kind of intramolecular tension). At this time, the π - π stacking effect between the benzene ring and the aromatic structure of anthracite in the surfactant was relatively obvious, but as the carbon chain becomes longer,

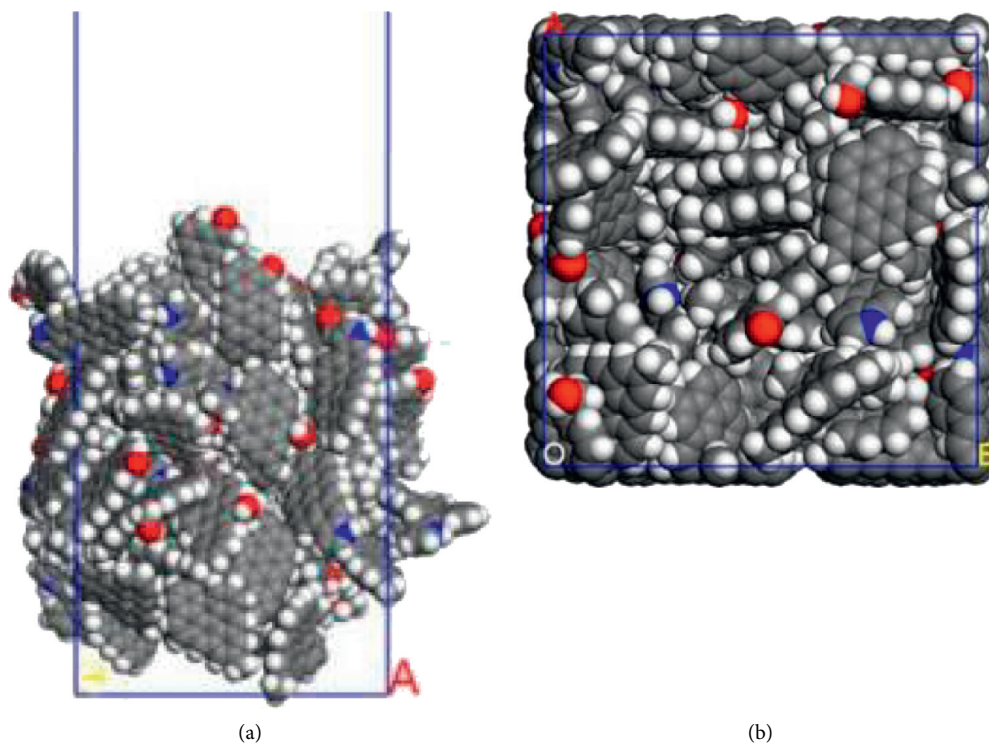


FIGURE 2: (a) Side view of the coal surface; (b) top view of the coal surface (the gray balls are carbon atoms, the red balls are oxygen atoms, the blue balls are nitrogen atoms, the white balls are hydrogen atoms, and the blue line is the model boundary).

this stacking effect weakens. The total adsorption energy showed a linear decreasing trend, which was the same as other previous studies. When $m = 12$, the adsorption energy was the most negative, indicating that the chain length had the greatest influence on the aggregation behavior of surfactants; at this time, under the combined effect of steric hindrance, hydrophobic interaction, and π - π stacking between the benzene ring and the aromatic structure of anthracite, the surfactant had the densest aggregation and the adsorption strength was higher than other systems. As the length of the hydrophobic carbon chain continued to increase, the intermolecular steric hindrance was enhanced, and the π - π stacking effect was weakened, which was not conducive to the aggregation of surfactant molecules, resulting in a linear increase in the total adsorption energy. At the same time, the hydrophobic interaction between the tail chain and the anthracite continued to increase. When $m = 18$, the influence of the hydrophobic interaction was dominant, causing the adsorption energy to decrease again.

The components of adsorption energy were further analyzed [54, 84, 87]. van der Waals interaction played a leading role in adsorption process, and electrostatic interaction was so small that it can be ignored. The range of electrostatic interaction was several nanometers [88]; although the simulation model satisfies the distance condition, due to the high degree of coalification of anthracite, low oxygen content, and low electronegativity, the charge difference between anthracite and anionic surfactant molecules was very small [89]. Therefore, the electrostatic interaction between the oppositely charged atoms was very weak.

3.1.2. Diffusion Coefficient. To describe the dynamics properties of the collector, the mean square displacement (MSD) was calculated. Based on the MSD, the diffusion coefficient (D) was calculated according to (2)–(4). A smaller diffusion coefficient value suggests higher dynamics properties [90].

$$\text{MSD} = \frac{1}{N} \sum_1^N [r_i(t) - r_i(0)]^2, \quad (2)$$

$$D = \frac{1}{6N} \lim_{t \rightarrow \infty} \frac{d}{dt} \sum_1^N [r_i(t) - r_i(0)]^2, \quad (3)$$

$$D = \lim_{t \rightarrow \infty} \left(\frac{\text{MSD}}{6t} \right) = \frac{1}{6} K, \quad (4)$$

where N is the total number of surfactant molecules; $r(t)$ and $r(0)$ are the position vectors of the surfactant molecules at time t and $t = 0$, respectively; K is the slope of the MSD curve; that is, the diffusion coefficient D is 1/6 of the slope of the MSD curve.

As seen from Figure 4, the change trend of the diffusion coefficient was the same as that of the adsorption energy. The diffusion coefficient of 12C was the smallest. This was because the 12C had the strongest adsorption strength on the anthracite surface model, which limited its free diffusion ability. This result was consistent with the adsorption energy and contact surface area results. The diffusion coefficient of 8C was much greater than that of other surfactants. This was due to the shortest hydrophobic carbon chain of 8C, which led to the smallest

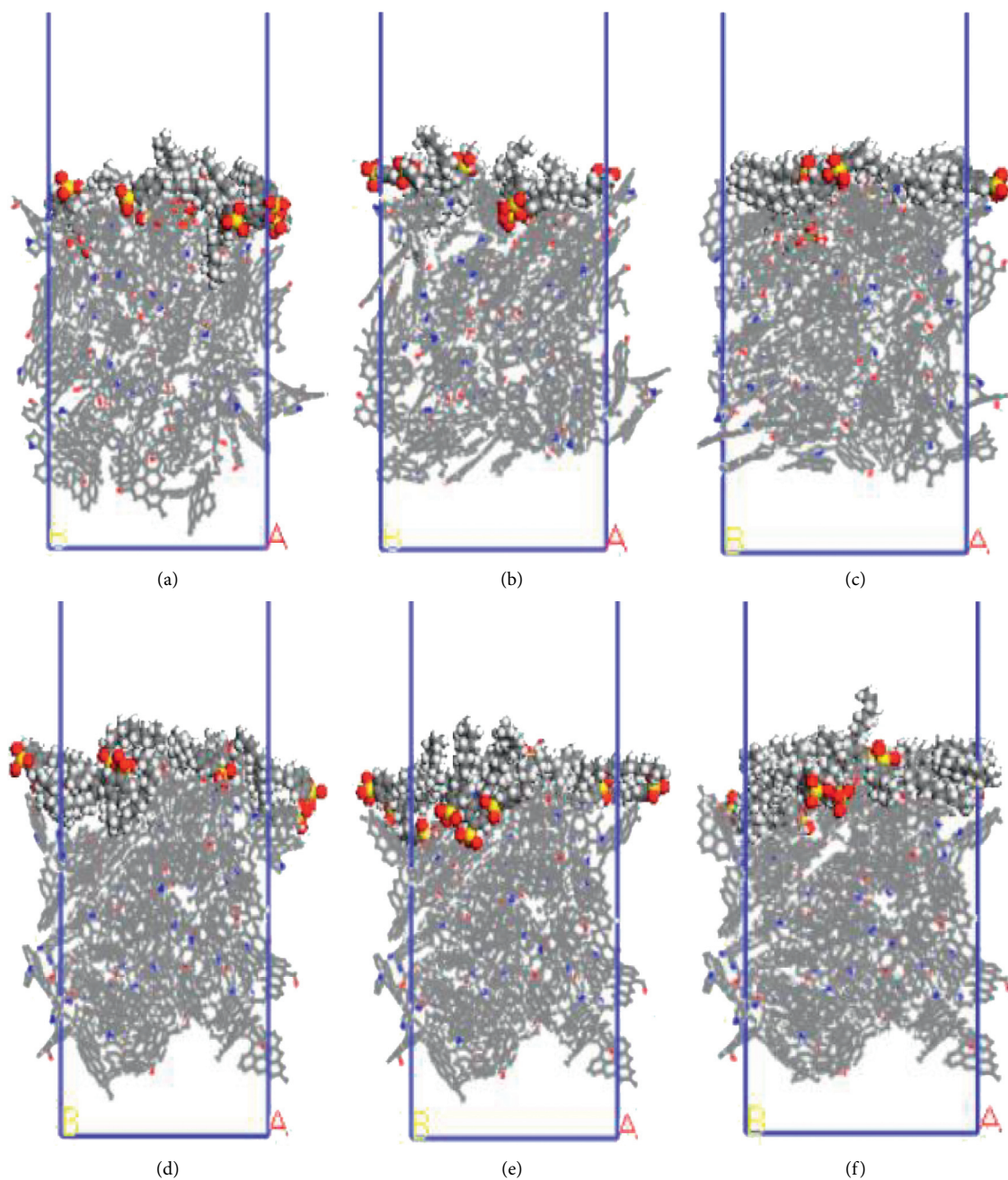


FIGURE 3: Equilibrium configuration of surfactant-anthracite system after MD simulation. (a) C8; (b) C10; (c) C12; (d) C14; (e) C16; (f) C18 (the yellow balls represent the sulfur atoms).

TABLE 3: Adsorption energy between surfactant and anthracite.

Model	EV (kcal·mol ⁻¹)	EL (kcal·mol ⁻¹)	E (kcal·mol ⁻¹)
8C-anthracite	-268.26	-3.34	-271.60
10C-anthracite	-290.06	-2.47	-290.53
12C-anthracite	-366.75	-5.51	-372.26
14C-anthracite	-269.37	-3.18	-272.55
16C-anthracite	-251.78	-3.84	-255.62
18C-anthracite	-266.59	-3.79	-270.38

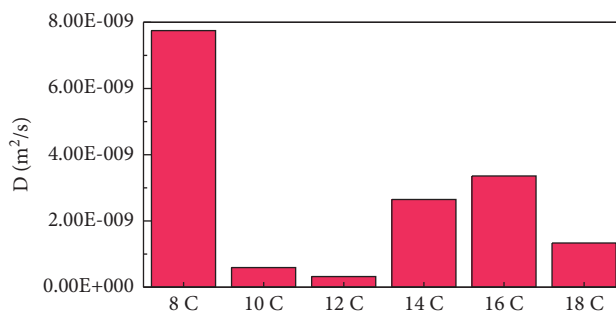


FIGURE 4: Diffusion coefficients of different systems.

hydrophobic interaction and the smallest intermolecular steric hindrance, resulting in the strongest free diffusion ability. This was consistent with the curvature analysis below.

3.2. Graphite Systems. Studies have found that oxygen-containing functional groups greatly affect the adsorption process [91]. In order to further explore the microscopic reasons for the highest adsorption strength of 12C on the surface of anthracite, the graphite layer was modified by hydroxyl and ketone groups, respectively.

Figure 5 shows models of the graphite layer modified by hydroxyl and ketone. The molecular structure of anthracite consists of an aromatic layer, which is very similar to the graphite flakes structure. Therefore, the surface of anthracite can be replaced by the surface of the graphite layer modified with oxygen-containing functional groups, which is more convenient and intuitive for the study of oxygen-containing functional groups [90, 92–96].

3.2.1. Adsorption Configuration. According to the construction method of the surfactant-anthracite system model in Section 2.1, 5 surfactant molecules were placed on the surface of the modified graphite layer, and the equilibrium was reached after 1000 ps molecular dynamics simulation. The final equilibrium configurations are shown in Figures 6 and 7.

3.2.2. Radial Distribution Function. The radial distribution function (RDF) between atoms can determine the degree of aggregation, and then by calculating the coordination number, the degree of aggregation of surfactants on the surface of anthracite can be quantified. The height of the first peak of RDF indicates the degree of order between atoms [25, 97–99]. The high and sharp peaks of RDF indicate strong order and strong interaction between atoms [100–104]. The radial distribution function was calculated by the following formula:

$$g(r) = \frac{1}{4\pi\rho_B r^2} \cdot \frac{dN}{dr}. \quad (5)$$

Figure 8 is the RDF between the oxygen atoms in the oxygen-containing group on the coal surface and the oxygen atoms in the surfactant.

As seen from Figure 8, the RDF peak of 12C was the highest near the coal surface hydroxyl groups, indicating that the interaction between 12C and coal surface hydroxyl groups was the strongest, and 12C aggregates most densely near the hydroxyl groups. The RDF peak of 12C near the ketone group on the coal surface was much higher than that of other surfactants, indicating that 12C also had the highest degree of aggregation near the ketone group. The RDF peak of 18C was the smallest near the ketone group and the hydroxyl group. This was because the 18C carbon chain was the longest, and the hydrophobic interaction between the hydrophobic carbon chain and anthracite was the strongest. At this time, the π - π stacking effect of the benzene ring and the aromatic structure of anthracite in the surfactant was the weakest. Although the steric effect was also the strongest at this time, according to the analysis of the adsorption energy, the hydrophobic interaction in 18C was dominant; this led to better interweaving of the hydrophobic tail chain with the coal surface, which made it more difficult for the oxygen atoms in the head group to contact with the oxygen-containing functional groups.

Generally, the coordination number refers to the number of B atoms around the A atom, which is a parameter for evaluating the strength of the interaction between atoms. Here, A represents the oxygen atoms in the oxygen-containing functional group, and B represents the oxygen atoms in the surfactants. The larger the value of the coordination number, the stronger the interaction between atoms. The coordination number was calculated by the following formula;

$$dN = \frac{g(r) \cdot N \cdot 4\pi r^2 dr}{V}. \quad (6)$$

In the formula, V is the periodic model volume and N is the total number of B atoms. Figure 9 shows the results.

The coordination number result was consistent with the RDF analysis result, and the coordination number could reflect the result more intuitively. The coordination number of 12C near the hydroxyl group was 1.36, which was much higher than that of other surfactants, and the coordination number near the ketone group was 0.93, which was much higher than other surfactants. It showed that 12C had the highest degree of aggregation near the hydroxyl group and the ketone group. The coordination number of 18C near the hydroxyl group was 0.52, and the coordination number near the ketone group was 0.36, both of which were the lowest.

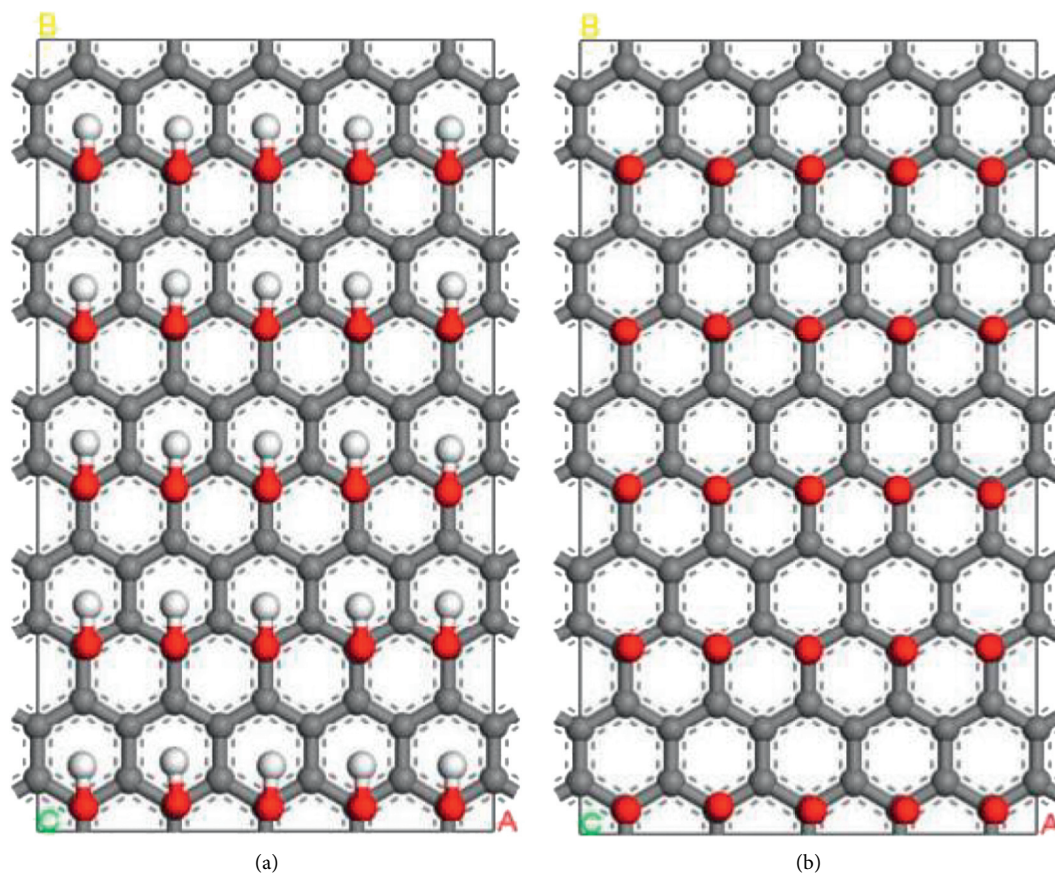


FIGURE 5: Graphite layer modified by oxygen-containing functional groups: (a) hydroxyl; (b) ketone.

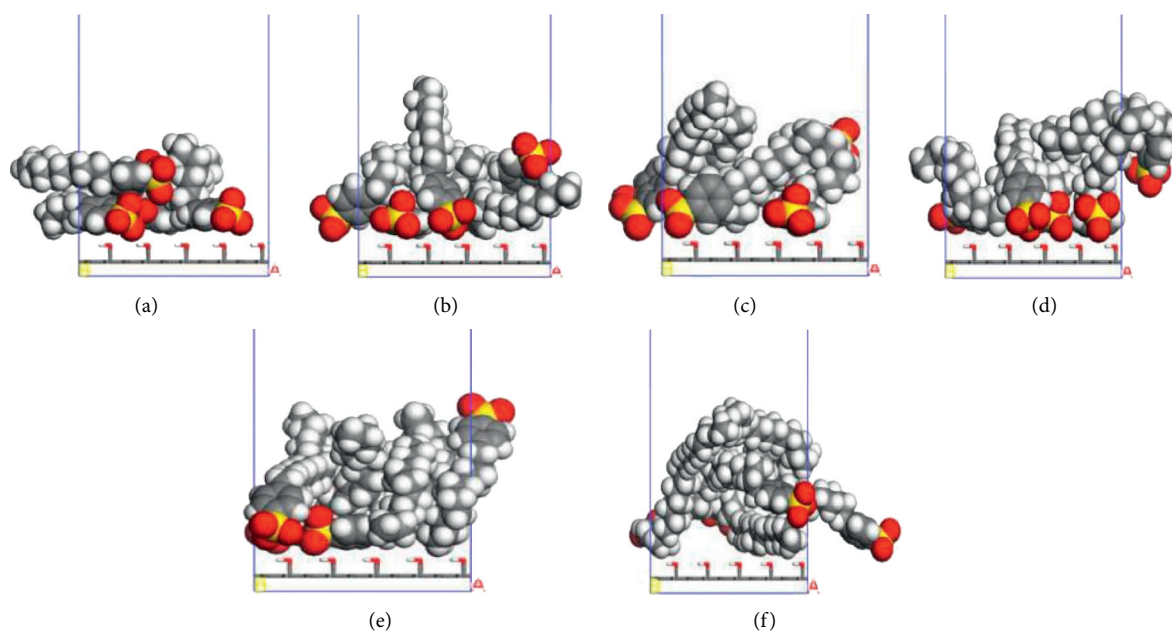


FIGURE 6: The final configuration of different systems adsorbed near the hydroxyl group: (a) C8; (b) C10; (c) C12; (d) C14; (e) C16; (f) C18.

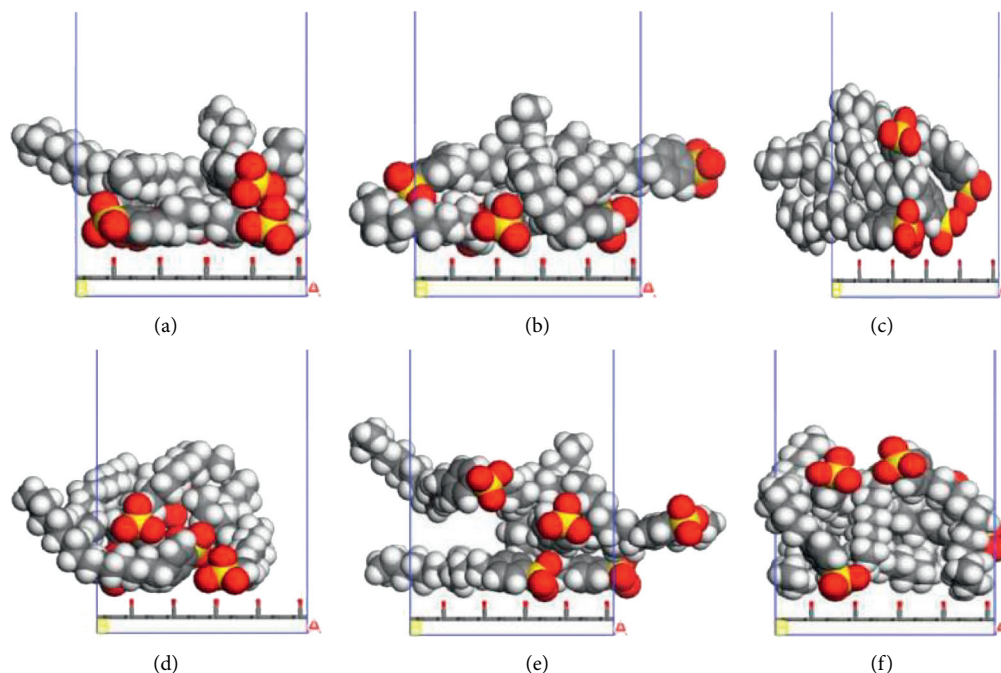


FIGURE 7: The final configuration of different systems adsorbed near the ketone group: (a) C8; (b) C10; (c) C12; (d) C14; (e) C16; (f) C18.

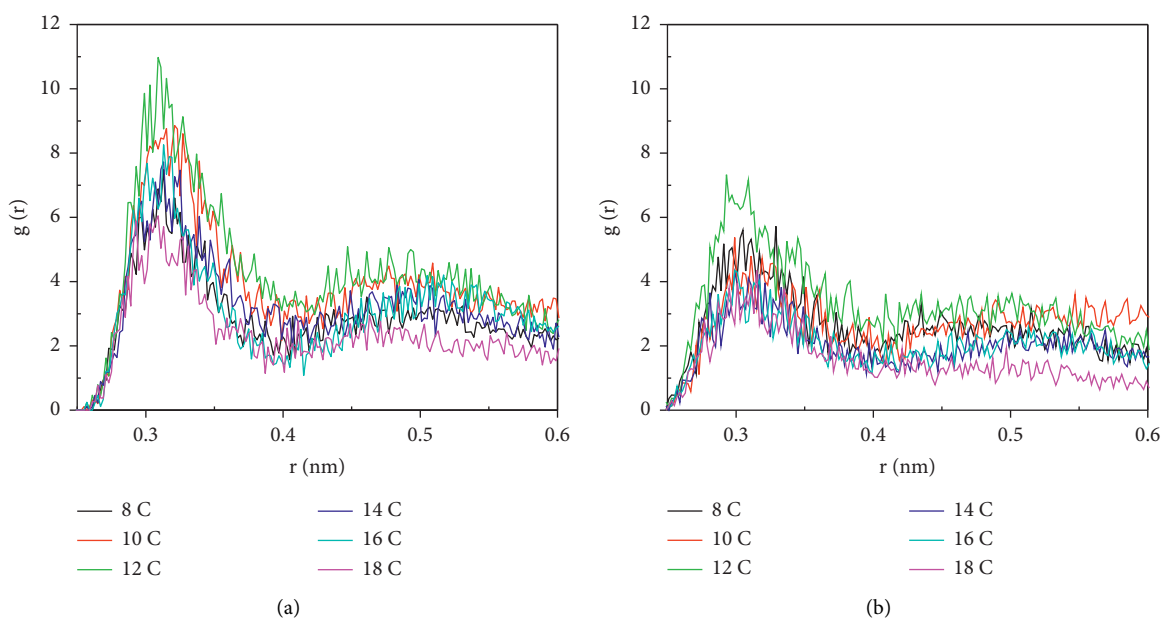


FIGURE 8: (a) The RDF of the oxygen atoms in the hydroxyl groups on the coal surface and the oxygen atoms in the surfactants; (b) the RDF of the oxygen atoms in the ketone groups on the coal surface and the oxygen atoms in the surfactants.

Through the abovementioned RDF and coordination number analysis, it was found that the reason for the highest degree of aggregation of 12C on the surface of anthracite was that it had the strongest ability to cover oxygen-containing functional groups on the surface of coal.

3.3. Water-Surfactant-Anthracite System. To further explore the compactness of the layered structure and the relationship between the diffusion characteristics of surfactants

in the aqueous solution, a water layer composed of 1,000 molecules was placed on the modified coal surface. After adding the water layer, the system became thermodynamically unstable. After the 1000 ps MD simulation, the system had regained equilibrium. Figure 10 shows the final conformation of the water-surfactant-anthracite system after MD simulation. After the surfactant layer covered the coal surface, it was equivalent to adding a water barrier layer [67]. The “isolation” effect made it difficult for water molecules to

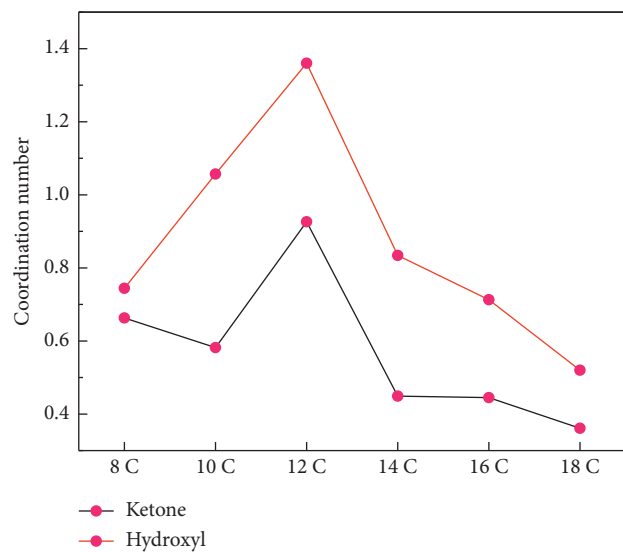


FIGURE 9: Coordination number of ketone group and hydroxyl group.

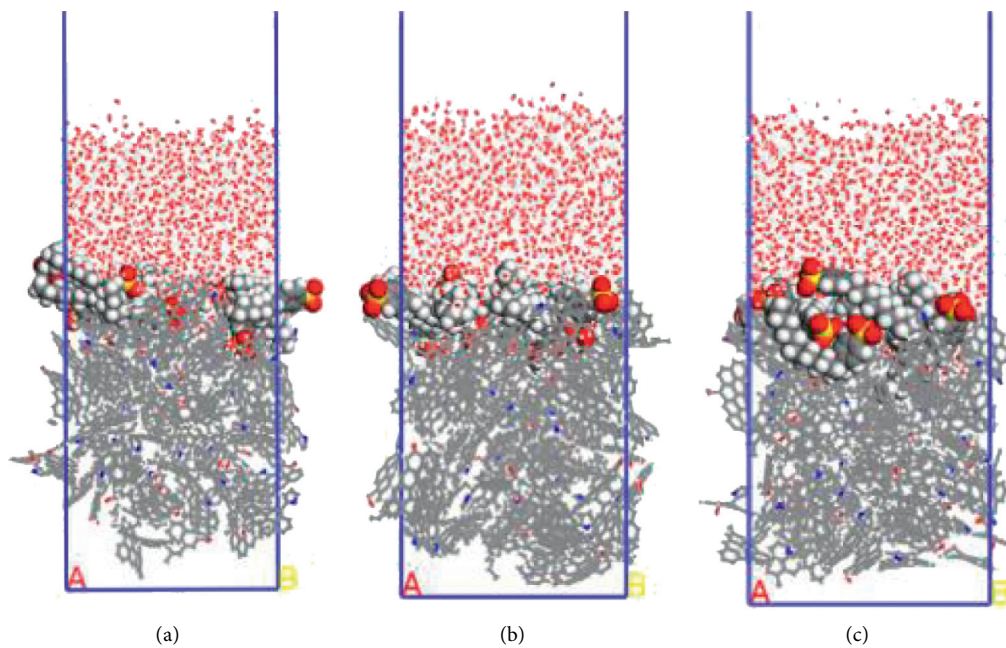


FIGURE 10: Continued.

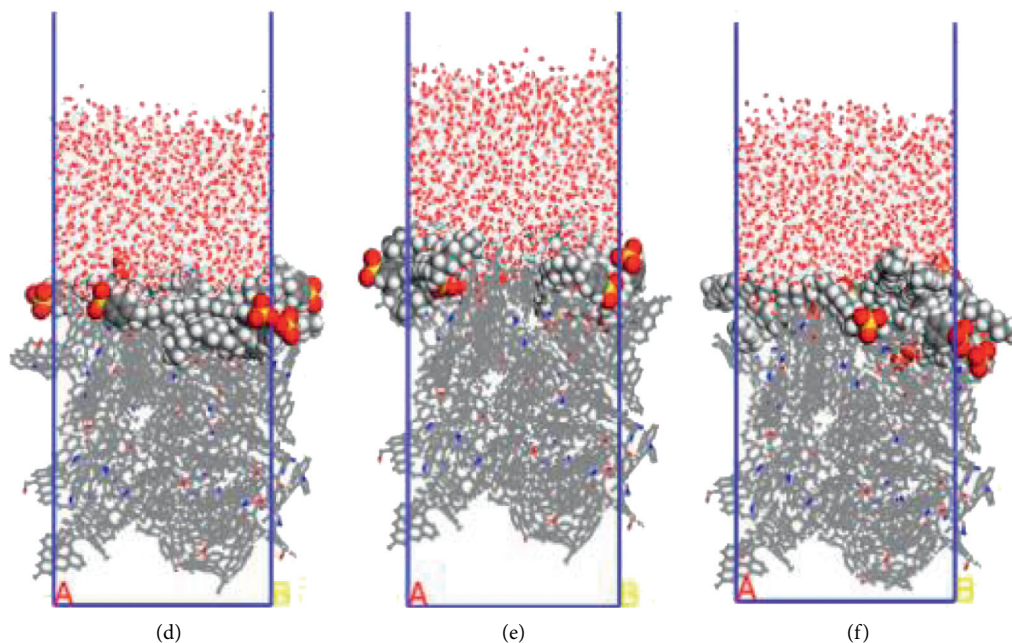


FIGURE 10: Equilibrium configuration of water-surfactant-anthracite system after MD simulation: (a) C8; (b) C10; (c) C12; (d) C14; (e) C16; (f) C18.

contact with anthracite. From Figure 10, the layered structure formed by 12C was the densest. The “isolation” ability of the layered structure to water molecules was used to evaluate the compactness of the layered structure. Furthermore, the microscopic reasons for the different degree of compactness of the layered structure were analyzed by the coordination number and RDF, the curvature of the hydrophobic tail chain, and the order parameters of the hydrophobic tail chain.

3.3.1. Radial Distribution Function. In order to determine the effect of the surfactant on the water molecules, the radial distribution function between the oxygen atoms ($O_w - O_w$) in the water molecules was calculated. As seen from Figure 11, the shape of the curve was not much different. Figure 11 showed that there was a peak between O_w atoms at about 0.29 nm, which was the average distance between oxygen atoms, but the peak heights were different. The RDF peak between O_w atoms in 12C was the lowest, indicating that the order of water molecules was the lowest in the system after 12C adsorption. It showed that the probability of finding O_w atoms around O_w atoms after 12C adsorption was the smallest at the same distance, indicating that the distance between O_w atoms was the largest. This was because the hydrophobic layer formed by 12C was the densest and had the strongest ability to “separate” the coal surface from the water layer, leading to more free diffusion of water molecules.

In order to compare the hydrophobic effect of the layered structure more intuitively, the coordination number between O_w was calculated, and the result is shown in Figure 12.

It can be seen that the coordination number of O_w after 12C adsorption was 10.07, which was the lowest among the six systems, which confirmed the above RDF conclusion. The change trend of coordination number was consistent with the above adsorption energy trend.

3.3.2. Hydrophobic Tail Order Parameters. The hydrophobic tail chain order parameter (S_{CD}) was used to measure the order of the hydrophobic tail chain, and then the adsorption strength of the hydrophobic tail chain on the surface of anthracite can be judged by calculation [23, 25, 72, 105]. S_{CD} was calculated using the following formula:

$$S_{CD} = \frac{1}{2} \langle 3 \cos^2 \theta - 1 \rangle. \quad (7)$$

θ was the angle between the hydrophobic tail chain and the Z axis. The order parameter could vary from $-1/2$ to 1. When the value of S_{CD} was 1, the hydrophobic tail chain was arranged along the vertical direction of the interface. When the value of S_{CD} was $-1/2$, the hydrophobic tail chains were arranged parallel to the interface. When $S_{CD} = 0$, the tail chain distribution was isotropic [72, 106, 107]. The order parameters of different systems are shown in Figure 13.

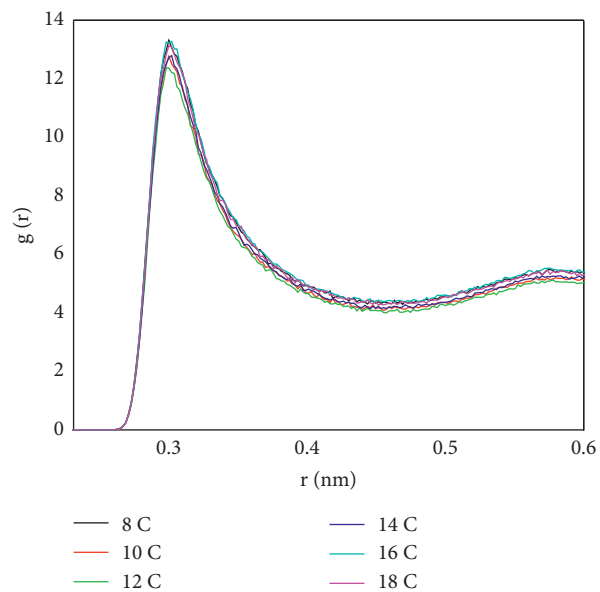


FIGURE 11: Radial distribution function between O_w and O_w .

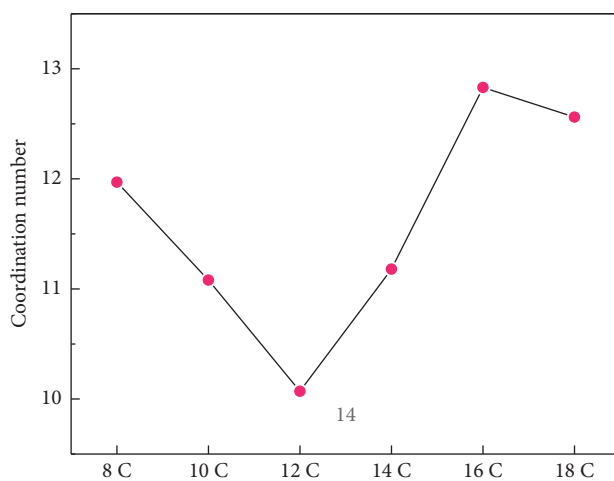


FIGURE 12: Coordination number of O_w .

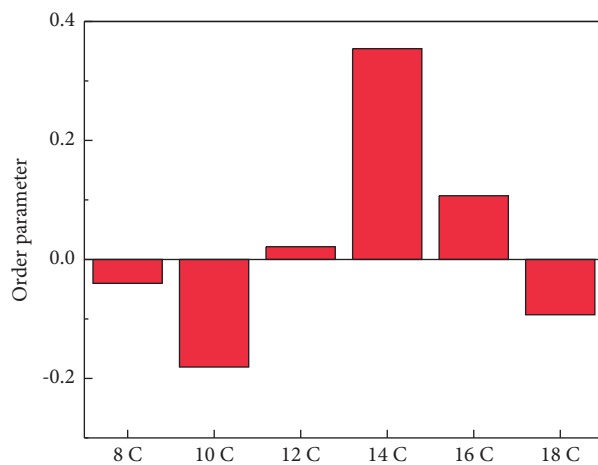


FIGURE 13: Order parameters of hydrophobic tails in different systems.

The S_{CD} value of 12C was the closest to zero, indicating that its isotropy was the strongest. This also allowed its molecules to be combined from different directions, so that the molecules could be better interwoven together to form a denser layered structure. The S_{CD} value of 10C was the smallest, indicating that its molecular chains tended to align along the interface; that is, the tendency to “lie flat” on the coal surface was the strongest. The S_{CD} value of 14C was the largest, indicating that its molecular chains tended to be arranged perpendicular to the coal surface, that is, “standing” on the coal surface.

4. Conclusions

MD simulation method was used to study the diffusion characteristics of six kinds of linear alkylbenzene sulfonates with different hydrophobic chain length on the surface of anthracite. After analysis, the following conclusions were drawn:

- (1) By analyzing the adsorption energy and diffusion coefficient of the surfactant-anthracite system, it was found that the total adsorption energy of the 12C/anthracite system was the lowest; the diffusion coefficient of 12C was the smallest. It showed that 12C had the highest adsorption strength on the surface of anthracite.
- (2) Through the analysis of coordination number and RDF in the surfactant-graphite layer system, it was found that the reason for the highest adsorption strength of 12C on the surface of anthracite was that it had the highest degree of aggregation near oxygen-containing functional groups on the surface of anthracite.
- (3) Through the analysis of the coordination number and RDF of the water oxygen atoms of the water-surfactant-anthracite system, it was found that the layered structure formed by 12C in the solution was the densest, and the ability to “isolate” water was the strongest. After further analysis of order parameters, it was found that the 12C order parameter was the closest to zero, indicating that its isotropy was the strongest, which also allows its molecules to be combined from different directions, better intertwined, forming a denser layered structure, and better covering the coal surface.
- (4) The systematic study of linear alkylbenzene sulfonates with different chain lengths on the surface of anthracite can better understand the influence of surfactant structure on the adsorption strength. This research fills the gap in the systematic study of the diffusion characteristics of LAS with different chain lengths on the surface of anthracite, expands the basic theory of wettability, and also provides ideas for the design and development of surfactants with new structures and new dust suppression agents.

Data Availability

The data used to support the findings of this study are included within the article.

Conflicts of Interest

The authors declare that there are no conflicts of interest regarding the publication of this paper.

Acknowledgments

This research was funded by the National Natural Science Foundation of China (Grant No. 51974195).

Supplementary Materials

Figures S1–S6: initial configuration of surfactant-anthracite system after MD simulation: S1: C8; S2: C10; S3: C12; S4: C14; S5: C16; S6: C18 (the purple sphere represents the sodium atom). (*Supplementary Materials*)

References

- [1] R. Y. Zhang, C. B. Sun, J. Kou, H. Zhao, D. Wei, and Y. Xing, “Enhancing the leaching of chalcopyrite using acidithiobacillus ferrooxidans under the induction of surfactant triton X-100,” *Minerals-Basel*, vol. 9, no. 1, 2019.
- [2] Z.-Y. Liu, C. Wang, H. Zhou et al., “Characterizing the impact of surfactant structure on interfacial tension: a molecular dynamics study,” *Journal of Molecular Modeling*, vol. 23, no. 4, 2017.
- [3] Y. S. Qiu, Y. F. Yu, L. Y. Zhang, Y. Qian, and Z. Ouyang, “An investigation of reverse flotation separation of sericite from graphite by using a surfactant: MF,” *Minerals-Basel*, vol. 6, no. 3, 2016.
- [4] P. Chen, Y. Hu, Z. Gao et al., “Discovery of a novel cationic surfactant: tributyltetradecyl-phosphonium chloride for iron ore flotation: from prediction to experimental verification,” *Minerals-Basel*, vol. 7, no. 12, 2017.
- [5] G. Huang, J. Xu, P. Geng, and J. Li, “Carrier flotation of low-rank coal with polystyrene [J],” *Minerals-Basel*, vol. 10, no. 5, 2020.
- [6] M. Winniewska, P. Nowicki, and T. Urban, “Influence of surfactants with different ionic character on the structure of poly(acrylic acid) adsorption layer on the activated bio-carbons surface—electrokinetic and stability studies,” *Journal of Molecular Liquids*, vol. 332, 2021.
- [7] T. Zhao, N. Feng, Y. Zhao, and C. Gong, “Adsorption properties and aggregation behavior of mixed system of anionic/cation surfactants with different structures,” *Journal of Molecular Liquids*, vol. 337, 2021.
- [8] J. Pei, X. Xing, B. Xia, Z. Wang, and Z. Luo, “Study on the adsorption behavior between an imidazolium ionic liquid and na-montmorillonite,” *Molecules*, vol. 24, no. 7, 2019.
- [9] I. C. Gifu, M. E. Maxim, L. O. Cinteza et al., “Antimicrobial activities of hydrophobically modified poly(acrylate) films and their complexes with different chain length cationic surfactants,” *Coatings*, vol. 9, no. 4, 2019.
- [10] Y. Xu, W. Huang, Q. Shi, Y. Zhang, J. Wu, and L. Song, “Porous nano-structured VO₂ films with different surfactants: synthesis mechanisms, characterization, and applications,” *Journal of Materials Science: Materials in Electronics*, vol. 24, no. 10, pp. 3823–3829, 2013.
- [11] C. Rupp, H. Steckel, and B. W. Muller, “Mixed micelle formation with phosphatidylcholines: the influence of surfactants with different molecule structures,” *International Journal of Pharmaceutics*, vol. 387, no. 1-2, pp. 120–128, 2010.

- [12] W. Wang, Y. Han, J. Zhu, Y. Fan, and Y. Wang, "Seeded growth of gold nanoparticles in aqueous solution of cationic gemini surfactants with different spacer length: influences of molecular and aggregate structures," *Journal of Nanoparticle Research*, vol. 21, no. 2, 2019.
- [13] H. Kim, B. Goh, S. Lee, K. Lee, and J. Choi, "Computational study on interfacial interactions between polymethyl methacrylate-based bone cement and hydroxyapatite in nanoscale [J]," *Applied Sciences-Basel*, vol. 11, no. 7, 2021.
- [14] S. Bai, J. Kubelka, and M. Piri, "Atomistic molecular dynamics simulations of surfactant-induced wettability alteration in crevices of calcite nanopores," *Energy & Fuels*, vol. 34, no. 3, pp. 3135–3143, 2020.
- [15] X. M. Yue, Z. Y. An, M. Ye et al., "Preparation of porous activated carbons for high performance supercapacitors from taixi anthracite by multi-stage activation," *Molecules*, vol. 24, no. 19, 2019.
- [16] Y. Liu, X. Ma, H. A. Li, and J. Hou, "Competitive adsorption behavior of hydrocarbon(s)/CO₂ mixtures in a double-nanopore system using molecular simulations," *Fuel*, vol. 252, pp. 612–621, 2019.
- [17] C. Yin, Y. Li, T. Zhang, J. Liu, Y. Yuan, and M. Huang, "Effects of exposure to anionic surfactants (SDBS and SDS) on nitrogen removal of aerobic denitrifier," *Water Environment Research*, vol. 92, no. 12, pp. 2129–2139, 2020.
- [18] C. Xu, D. Wang, H. Wang et al., "Experimental investigation of coal dust wetting ability of anionic surfactants with different structures," *Process Safety and Environmental Protection*, vol. 121, pp. 69–76, 2019.
- [19] A. Askari, F. Vahabzadeh, and M. M. Mardanpour, "Quantitative determination of linear alkylbenzene sulfonate (LAS) concentration and simultaneous power generation in a microbial fuel cell-based biosensor," *Journal of Cleaner Production*, vol. 294, 2021.
- [20] X. Zhao, L. Gong, G. Liao et al., "Micellar solubilization of petroleum fractions by heavy alkylbenzene sulfonate surfactant," *Journal of Molecular Liquids*, vol. 329, 2021.
- [21] L. Franco-Belussi, M. Jones-Costa, R. F. Salla et al., "Hepatotoxicity of the anionic surfactant linear alkylbenzene sulphonate (LAS) in bullfrog tadpoles," *Chemosphere*, vol. 266, 2021.
- [22] X. He, W. Shinoda, R. Devane, K. L. Anderson, and M. L. Klein, "Paramaterization of a coarse-grained model for linear alkylbenzene sulfonate surfactants and molecular dynamics studies of their self-assembly in aqueous solution," *Chemical Physics Letters*, vol. 487, no. 1–3, pp. 71–76, 2010.
- [23] K. Takeda, Y. Andoh, W. Shinoda, and S. Okazaki, "Molecular behavior of linear alkylbenzene sulfonate in hydrated crystal, tilted gel, and liquid crystal phases studied by molecular dynamics simulation," *Langmuir*, vol. 35, no. 33, pp. 10877–10884, 2019.
- [24] L. Chai, L. Yang, Y. Zhang, Y. Zhou, F. Wang, and Z. Wu, "Antagonism or synergism? responses of hydrocharis dubia (Bl.) Backer to linear alkylbenzene sulfonate, naphthalene and their joint exposure," *Ecotoxicology and Environmental Safety*, vol. 200, 2020.
- [25] X. He, O. Guvench, A. D. Mackerell JR., and M. L. Klein, "Atomistic simulation study of linear alkylbenzene sulfonates at the water/air interface," *The Journal of Physical Chemistry B*, vol. 114, no. 30, pp. 9787–9794, 2010.
- [26] G. A. Smith, A. Huggett, C. Jones, and G. Ortego, "Surface activity and performance properties of gemini salts of linear alkylbenzene sulfonate in aqueous solution," *Journal of Surfactants and Detergents*, vol. 24, no. 4, pp. 563–574, 2021.
- [27] T. Lee, U. Park, P. Puligundla, and C. Mok, "Corona discharge plasma-based degradation of simulated residual linear alkylbenzene sulphonate and dodecyl benzene sulfonate surfactants," *International Journal of Environmental Science and Technology*, vol. 17, no. 2, pp. 1171–1178, 2020.
- [28] N. Kishimoto and S. Hamamoto, "Removal of linear alkylbenzene sulfonate (LAS) by a cetyltrimethylammonium bromide (CTAB)-aided coagulation-filtration process," *Environmental Technology*, vol. 43, no. 6, pp. 815–823, 2020.
- [29] X. Wang, X. Liu, Y. Huo, and J. Niu, "Properties of binary mixture of cetyl diphenyl ether disulfonate and linear alkylbenzene sulfonate," *Tenside Surfactants Detergents*, vol. 57, no. 3, pp. 259–264, 2020.
- [30] E. Koohsaryan, M. Anbia, M. Sepehrian, and M. Maghsoodlu, "Facile hydrothermal synthesis of hierarchical sodium P zeolite as a nonphosphate detergent builder," *Journal of Surfactants and Detergents*, vol. 24, no. 1, pp. 85–97, 2021.
- [31] H. Z. Gang, P. C. Bian, X. He et al., "Mixing of surfactin, an anionic biosurfactant, with alkylbenzene sulfonate, a chemically synthesized anionic surfactant, at the *n*-decane/water interface," *Journal of Surfactants and Detergents*, vol. 24, no. 3, pp. 445–457, 2021.
- [32] H.-Y. Cai, Y. Zhang, Z.-Y. Liu et al., "Molecular dynamics simulation of binary betaine and anionic surfactant mixtures at decane–water interface," *Journal of Molecular Liquids*, vol. 266, pp. 82–89, 2018.
- [33] X. DU, L. Zhao, X. He, H. Chen, W. Fang, and W. Li, "Ultra-stable aqueous foams with multilayer films stabilized by 1-dodecanol, sodium dodecyl sulfonate and polyvinyl alcohol," *Chemical Engineering Science*, vol. 160, pp. 72–79, 2017.
- [34] Z. Liu, G. Zhou, S. Li, C. Wang, R. Liu, and W. Jiang, "Molecular dynamics simulation and experimental characterization of anionic surfactant: influence on wettability of low-rank coal," *Fuel*, vol. 279, 2020.
- [35] W. Han, G. Zhou, M. Xing et al., "Experimental investigation on physicochemical characteristics of coal treated with synthetic sodium salicylate-imidazole ionic liquids," *Journal of Molecular Liquids*, vol. 327, 2021.
- [36] B. Li, S. Liu, J. Guo, L. Zhang, and X. Sun, "Increase in wettability difference between organic and mineral matter to promote low-rank coal flotation by using ultrasonic treatment," *Applied Surface Science*, vol. 481, pp. 454–459, 2019.
- [37] L. Li, M. He, Z. Li, C. Ma, H. Yu, and X. You, "Wettability effect of ethoxylated nonyl phenol with different ethylene oxide chain length on shendong long-flame coal surface," *Materials Today Communications*, vol. 26, 2021.
- [38] J. Meng, F. Yin, S. Li, R. Zhong, Z. Sheng, and B. Nie, "Effect of different concentrations of surfactant on the wettability of coal by molecular dynamics simulation," *International Journal of Mining Science and Technology*, vol. 29, no. 4, pp. 577–584, 2019.
- [39] B. Liu, Y. Zhang, K. Xu, Y. Zhang, Z. Hao, and N. Ma, "Study on a new type of composite powder explosion inhibitor used to suppress underground coal dust explosion," *Applied Sciences-Basel*, vol. 11, no. 18, 2021.
- [40] C. L. Oproiu, G. Voicu, A. Bădănoiu, and A. I. Nicoră, "The solidification/stabilization of wastewater (from a landfill leachate) in specially designed binders based on coal ash," *Materials*, vol. 14, no. 19, 2021.
- [41] H. Jin, Y. Zhang, K. Chen et al., "Preparation and characterization of a composite dust suppressant for coal mines," *Polymers-Basel*, vol. 12, no. 12, 2020.

- [42] M. Yuan, W. Nie, W. Zhou et al., "Determining the effect of the non-ionic surfactant AEO(9) on lignite adsorption and wetting via molecular dynamics (MD) simulation and experiment comparisons," *Fuel*, vol. 278, 2020.
- [43] B. Li, S. Liu, M. Fan, and L. Zhang, "The effect of ethylene oxide groups in dodecyl ethoxyl ethers on low rank coal flotation: an experimental study and simulation," *Powder Technology*, vol. 344, pp. 684–692, 2019.
- [44] H. Zhang, P. XI, Q. Zhuo, and W. Liu, "Construction of molecular model and adsorption of collectors on bulianta coal," *Molecules*, vol. 25, no. 17, 2020.
- [45] H. Chang, H. Zhang, Z. Jia, X. Li, W. Gao, and W. Wei, "Wettability of coal pitch surface by aqueous solutions of cationic gemini surfactants," *Colloids and Surfaces A: Physicochemical and Engineering Aspects*, vol. 494, pp. 59–64, 2016.
- [46] X. Liu, S. Liu, Y. Cheng, and G. Xu, "Decrease in hydrophilicity and moisture re-adsorption of lignite: effects of surfactant structure," *Fuel*, vol. 273, 2020.
- [47] G. Ni, S. Qian, X. Meng et al., "Effect of NaCl-SDS compound solution on the wettability and functional groups of coal," *Fuel*, vol. 257, 2019.
- [48] Q. Yao, C. Xu, Y. Zhang, G. Zhou, S. Zhang, and D. Wang, "Micromechanism of coal dust wettability and its effect on the selection and development of dust suppressants," *Process Safety and Environmental Protection*, vol. 111, pp. 726–732, 2017.
- [49] Z. Chang, X. Chen, and Y. Peng, "The interaction between diesel and surfactant triton X-100 and their adsorption on coal surfaces with different degrees of oxidation," *Powder Technology*, vol. 342, pp. 840–847, 2019.
- [50] X. Liu, S. Liu, M. Fan, and L. Zhang, "Decrease of hydrophilicity of lignite using CTAB: effects of adsorption differences of surfactant onto mineral composition and functional groups," *Fuel*, vol. 197, pp. 474–481, 2017.
- [51] H. Chen, A. Gizzatov, and A. I. Abdel-Fattah, "Molecular assembly of surfactant mixtures in oil-swollen micelles: implications for high salinity colloidal stability," *The Journal of Physical Chemistry B*, vol. 124, no. 3, pp. 568–576, 2020.
- [52] J. Zhou and P. G. Ranjith, "Self-assembly and viscosity changes of binary surfactant solutions: a molecular dynamics study," *Journal of Colloid and Interface Science*, vol. 585, pp. 250–257, 2021.
- [53] P. Müller, D. J. Bonhuis, R. Miller, and E. Schneck, "Ionic surfactants at air/water and oil/water interfaces: a comparison based on molecular dynamics simulations," *The Journal of Physical Chemistry B*, vol. 125, no. 1, pp. 406–415, 2021.
- [54] J. Kubelka, S. Bai, and M. Piri, "Effects of surfactant charge and molecular structure on wettability alteration of calcite: insights from molecular dynamics simulations," *The Journal of Physical Chemistry B*, vol. 125, no. 4, pp. 1293–1305, 2021.
- [55] L. Zhang, Z. Liu, T. Ren et al., "Understanding the structure of hydrophobic surfactants at the air/water interface from molecular level," *Langmuir*, vol. 30, no. 46, pp. 13815–13822, 2014.
- [56] B. Saha, A. Sankar Patra, A. K. Mukherjee, and I. Paul, "Interaction and thermal stability of carboxymethyl cellulose on α -Fe₂O₃(001) surface: ReaxFF molecular dynamics simulations study," *Journal of Molecular Graphics and Modelling*, vol. 102, 2021.
- [57] B. Li, S. Liu, J. Guo, and L. Zhang, "Interaction between low rank coal and kaolinite particles: a DFT simulation," *Applied Surface Science*, vol. 456, pp. 215–220, 2018.
- [58] H. Domínguez, "Computer studies on the effects of long chain alcohols on sodium dodecyl sulfate (SDS) molecules in SDS/dodecanol and SDS/hexadecanol monolayers at the air/water interface," *The Journal of Physical Chemistry B*, vol. 110, no. 26, pp. 13151–13157, 2006.
- [59] L. Wang, N. Sun, Z. Wang et al., "Self-assembly of mixed dodecylamine-dodecanol molecules at the air/water interface based on large-scale molecular dynamics," *Journal of Molecular Liquids*, vol. 276, pp. 867–874, 2019.
- [60] M. Wang, J. Gao, J. Xu, Q. Du, and Y. Zhang, "Effect of H₂O on the transformation of sulfur during demineralized coal pyrolysis: molecular dynamics simulation using ReaxFF," *Energy & Fuels*, vol. 35, no. 3, pp. 2379–2390, 2021.
- [61] M. Hao, Z. Qiao, H. Zhang, Y. Wang, and Y. Li, "Thermodynamic analysis of CH₄/CO₂/N₂ adsorption on anthracite coal: investigated by molecular simulation," *Energy & Fuels*, vol. 35, no. 5, pp. 4246–4257, 2021.
- [62] K. Dong, F. Zeng, J. Jia, C. Chen, and Z. Gong, "Molecular simulation of the preferential adsorption of CH₄ and CO₂ in middle-rank coal," *Molecular Simulation*, vol. 45, no. 1, pp. 15–25, 2019.
- [63] S. Yu, J. Bo, and Q. Meijun, "Molecular dynamic simulation of self- and transport diffusion for CO₂/CH₄/N₂ in low-rank coal vitrinite," *Energy & Fuels*, vol. 32, no. 3, pp. 3085–3096, 2018.
- [64] Y. Li, Z. Yang, and X. Li, "Molecular simulation study on the effect of coal rank and moisture on CO₂/CH₄ competitive adsorption," *Energy & Fuels*, vol. 33, no. 9, pp. 9087–9098, 2019.
- [65] R. Chen, X. Dong, Y. Fan, X. Ma, Y. Dong, and M. Chang, "Interaction between STAC and coal/kaolinite in tailing dewatering: an experimental and molecular-simulation study," *Fuel*, vol. 279, 2020.
- [66] X. M. Ma, Y. P. Fan, and X. S. Dong, "Impact of clay minerals on the dewatering of coal slurry: an experimental and molecular-simulation study," *Minerals-Basel*, vol. 8, no. 9, 2018.
- [67] L. Zhang, B. Li, Y. Xia, and S. Liu, "Wettability modification of wender lignite by adsorption of dodecyl poly ethoxylated surfactants with different degree of ethoxylation: a molecular dynamics simulation study," *Journal of Molecular Graphics and Modelling*, vol. 76, pp. 106–117, 2017.
- [68] B. Li, J. Guo, S. Liu, B. Albijanic, L. Zhang, and X. Sun, "Molecular insight into the mechanism of benzene ring in nonionic surfactants on low-rank coal floatability," *Journal of Molecular Liquids*, vol. 302, 2020.
- [69] J. Guo, Y. Xia, Y. Liu, S. Liu, L. Zhang, and B. Li, "Microscopic adsorption behaviors of ionic surfactants on lignite surface and its effect on the wettability of lignite: a simulation and experimental study," *Journal of Molecular Liquids*, vol. 345, 2022.
- [70] C. Xuanlai, G. Yan, X. Yang, and G. Xu, "Study on adsorption characteristics of sulfonate gemini surfactant on lignite surface," *Minerals-Basel*, vol. 11, no. 12, 2021.
- [71] X. L. Chen, G. C. Yan, and X. L. Yang, "Microscopic diffusion characteristics of linear alkylbenzene sulfonates on the surface of anthracite: the influence of different attachment sites of benzene ring in the backbone [J]," *Minerals-Basel*, vol. 11, no. 10, 2021.
- [72] L. S. Vermeer, B. L. DE Groot, V. Réat, A. Milon, and J. Czaplicki, "Acyl chain order parameter profiles in phospholipid bilayers: computation from molecular dynamics simulations and comparison with 2H NMR

- experiments,” *European Biophysics Journal*, vol. 36, no. 8, pp. 919–931, 2007.
- [73] O. Acisli, S. Karaca, and A. Gurses, “Investigation of the alkyl chain lengths of surfactants on their adsorption by montmorillonite (Mt) from aqueous solutions,” *Applied Clay Science*, vol. 142, pp. 90–99, 2017.
- [74] H.-P. Ren, S.-P. Tian, M. Zhu et al., “Modification of montmorillonite by gemini surfactants with different chain lengths and its adsorption behavior for methyl orange,” *Applied Clay Science*, vol. 151, pp. 29–36, 2018.
- [75] R. Kun, L. Kis, and I. Dékány, “Hydrophobization of bovine serum albumin with cationic surfactants with different hydrophobic chain length,” *Colloids and Surfaces B: Biointerfaces*, vol. 79, no. 1, pp. 61–68, 2010.
- [76] Y. Jiang, T. Geng, Q. Li, G. Li, and H. Ju, “Equilibrium and dynamic surface tension properties of salt-free catanionic surfactants with different hydrocarbon chain lengths,” *Journal of Molecular Liquids*, vol. 204, pp. 126–131, 2015.
- [77] A. M. Diez-Pascual, C. Vallés, R. Mateos, S. Vera-López, I. A. Kinloch, and M. P. S. Andrés, “Influence of surfactants of different nature and chain length on the morphology, thermal stability and sheet resistance of graphene,” *Soft Matter*, vol. 14, no. 29, pp. 6013–6023, 2018.
- [78] H. Zhang, M. Xia, F. Wang, P. Li, and M. Shi, “Adsorption properties and mechanism of montmorillonite modified by two gemini surfactants with different chain lengths for three benzotriazole emerging contaminants: experimental and theoretical study,” *Applied Clay Science*, vol. 207, 2021.
- [79] L. Badache, Z. Lehanine, and W. Naït Abderrahmane, “Synthesis and surface properties study of a series of cationic surfactants with different hydrophobic chain lengths,” *Journal of Surfactants and Detergents*, vol. 15, no. 6, pp. 715–720, 2012.
- [80] S. Wei, G. C. Yan, Z. Q. Zhang, M. S. Liu, and Y. F. Zhang, “Molecular structure analysis of jincheng anthracite coal,” *Journal of China Coal Society*, vol. 43, no. 2, pp. 555–562, 2018.
- [81] Z. Zhang, C. Wang, and K. Yan, “Adsorption of collectors on model surface of wiser bituminous coal: a molecular dynamics simulation study,” *Minerals Engineering*, vol. 79, pp. 31–39, 2015.
- [82] X. You, M. He, W. Zhang et al., “Molecular dynamics simulations of nonylphenol ethoxylate on the hatcher model of subbituminous coal surface,” *Powder Technology*, vol. 332, pp. 323–330, 2018.
- [83] R. Zhang, Y. Xing, Y. Xia et al., “New insight into surface wetting of coal with varying coalification degree: an experimental and molecular dynamics simulation study,” *Applied Surface Science*, vol. 511, 2020.
- [84] Y. Xia, Z. Yang, R. Zhang, Y. Xing, and X. Gui, “Enhancement of the surface hydrophobicity of low-rank coal by adsorbing DTAB: an experimental and molecular dynamics simulation study,” *Fuel*, vol. 239, pp. 145–152, 2019.
- [85] J. Li, Y. Han, G. Qu et al., “Molecular dynamics simulation of the aggregation behavior of N-dodecyl-N, N-dimethyl-3-ammonio-1-propanesulfonate/sodium dodecyl benzene sulfonate surfactant mixed system at oil/water interface,” *Colloids and Surfaces A: Physicochemical and Engineering Aspects*, vol. 531, pp. 73–80, 2017.
- [86] M. H. Anvari, Q. Liu, Z. Xu, and P. Choi, “Molecular dynamics study of hydrophilic sphalerite (110) surface as modified by normal and branched butylthiols,” *Langmuir*, vol. 34, no. 10, pp. 3363–3373, 2018.
- [87] J. Guo, L. Zhang, S. Liu, and B. Li, “Effects of hydrophilic groups of nonionic surfactants on the wettability of lignite surface: molecular dynamics simulation and experimental study,” *Fuel*, vol. 231, pp. 449–457, 2018.
- [88] Q. Liu, S. Yuan, H. Yan, and X. Zhao, “Mechanism of oil detachment from a silica surface in aqueous surfactant solutions: molecular dynamics simulations,” *The Journal of Physical Chemistry B*, vol. 116, no. 9, pp. 2867–2875, 2012.
- [89] X. He, X. Liu, D. Song, and B. Nie, “Effect of microstructure on electrical property of coal surface,” *Applied Surface Science*, vol. 483, pp. 713–720, 2019.
- [90] L. Zhang, X. L. Sun, B. Li, Z. Xie, J. Guo, and S. Liu, “Experimental and molecular dynamics simulation study on the enhancement of low rank coal flotation by mixed collector,” *Fuel*, vol. 266, 2020.
- [91] W. Wang, L. Liang, Y. Peng, and M. Holuszko, “Surface chemical heterogeneity of low rank coal characterized by micro-FTIR and its correlation with hydrophobicity,” *Minerals-Basel*, vol. 11, no. 3, 2021.
- [92] L. Zhang, J. Guo, M. Hao, B. Li, and S. Liu, “Microscopic spreading characteristics of non-polar oil droplet on low rank coal surface: effects of surfactant pretreatment and oxygen-containing groups,” *Journal of Molecular Liquids*, vol. 325, 2021.
- [93] S. Zhang, B. Song, C. Cao et al., “Structural evolution of high-rank coals during coalification and graphitization: X-ray diffraction, Raman spectroscopy, high-resolution transmission electron microscopy, and reactive force field molecular dynamics simulation study,” *Energy & Fuels*, vol. 35, no. 3, pp. 2087–2097, 2021.
- [94] X. Ma, X. Dong, and Y. Fan, “Prediction and characterization of the microcrystal structures of coal with molecular simulation,” *Energy & Fuels*, vol. 32, no. 3, pp. 3097–3107, 2018.
- [95] M. Gao, X. Li, C. Ren, Z. Wang, Y. Pan, and L. Guo, “Construction of a multicomponent molecular model of fugu coal for ReaxFF-MD pyrolysis simulation,” *Energy & Fuels*, vol. 33, no. 4, pp. 2848–2858, 2019.
- [96] J. Bian, X. Li, F. Zeng, and X. Wang, “Construction and evaluation of a medium-rank coal molecular model using a hybrid experimental-simulation-theoretical method,” *Energy & Fuels*, vol. 33, no. 12, pp. 12905–12915, 2019.
- [97] H. Yan, X.-L. Guo, S.-L. Yuan, and C.-B. Liu, “Molecular dynamics study of the effect of calcium ions on the monolayer of SDC and SDSn surfactants at the vapor/liquid interface,” *Langmuir*, vol. 27, no. 10, pp. 5762–5771, 2011.
- [98] J.-S. Yang, C.-L. Yang, M.-S. Wang, B.-D. Chen, and X.-G. Ma, “Crystallization of alkane melts induced by carbon nanotubes and graphene nanosheets: a molecular dynamics simulation study,” *Physical Chemistry Chemical Physics*, vol. 13, no. 34, pp. 15476–15482, 2011.
- [99] T. Zhao, G. Xu, S. Yuan, Y. Chen, and H. Yan, “Molecular dynamics study of alkyl benzene sulfonate at air/water interface: effect of inorganic salts,” *The Journal of Physical Chemistry B*, vol. 114, no. 15, pp. 5025–5033, 2010.
- [100] A. G. Guruge, D. B. Warren, H. Benameur, C. W. Pouton, and D. K. Chalmers, “Aqueous phase behavior of the PEO-containing non-ionic surfactant C12E6: a molecular dynamics simulation study,” *Journal of Colloid and Interface Science*, vol. 588, pp. 257–268, 2021.
- [101] J. Xu, Y. Zhang, H. Chen et al., “Effect of surfactant head-groups on the oil/water interface: an interfacial tension measurement and simulation study,” *Journal of Molecular Structure*, vol. 1052, pp. 50–56, 2013.

- [102] J. G. Parra, H. Domínguez, Y. Aray, P. Iza, X. Zarate, and E. Schott, "Behavior of the SDS/1-butanol and SDS/2-butanol mixtures at the water/*n*-octane interface through molecular dynamics simulations," *Chemical Physics*, vol. 523, pp. 138–149, 2019.
- [103] J. G. Parra, H. Dominguez, and Y. Aray, "Structural and interfacial properties of the CO₂-in-water foams prepared with sodium dodecyl sulfate (SDS): a molecular dynamics simulation study," *Colloid Surface A*, vol. 578, Article ID 123, 2019.
- [104] L. Wang, Y. Hu, R. Liu, J. Liu, and W. Sun, "Synergistic adsorption of DDA/alcohol mixtures at the air/water interface: a molecular dynamics simulation," *Journal of Molecular Liquids*, vol. 243, pp. 1–8, 2017.
- [105] T. B. Stanishneva-Konovalova and O. S. Sokolova, "Molecular dynamics simulations of negatively charged DPPC/DPPI lipid bilayers at two levels of resolution," *Computational and Theoretical Chemistry*, vol. 1058, pp. 61–66, 2015.
- [106] F. Rodríguez-Roperó and M. Fioroni, "Effect of Na⁺, Mg²⁺, and Zn²⁺ chlorides on the structural and thermodynamic properties of water/*n*-heptane interfaces," *Journal of Computational Chemistry*, vol. 32, no. 9, pp. 1876–1886, 2011.
- [107] H. Sun, H. Xiao, and X. Liu, "Structural properties of hydroxyl-substituted alkyl benzenesulfonates at the water/vapor and water/decane interfaces," *Science China Chemistry*, vol. 54, no. 7, pp. 1078–1085, 2011.